Materials and Manufacturing Processes, 27: 1429–1436, 2012

ISSN: 1042-6914 print/1532-2475 online
DOI: 10.1080/10426914.2012.709340

Taylor & Francis
Taylor & Francis Group

Heterogeneous Friction Stir Welding: Improved Properties in Dissimilar Aluminum Alloy Joints through Insertion of Copper Coupled with External Heating

J. Kandasamy[1], M. Manzoor Hussain[2], and S. Rajesham[3]

[1]*Department of Mechanical Engineering, MVSR Engineering College, Nadergul, Hyderabad, India*
[2]*Department of Mechanical Engineering, College of Engineering, JNTUH, Hyderabad, India*
[3]*Pulla Reddy Institute of Technology, Wargal, Medak District, Andhrapradesh, India*

Friction stir welding (FSW) experiments are conducted on AA7075 and AA6061 alloys under optimized conditions with copper as intermediate inclusion on the faying sides of the base material assisted by external heating from the root side during the process. The concept behind the experimentation is to minimize the temperature gradient that exists between the top and bottom sides of the plates. The work attempts to relocate the crack initiation point from the root of the retreating side, as in conventional friction stir weldments due to the variation in material flow along the weld cross-section. Analysis of the formed intermetallic compound (IMC) indicates that the interaction of AA7075, AA6061 alloys with copper, in coating form, enhances the bond strength by formation of Al_2Cu and Al_4Cu_9 IMCs. High thermal conductivity of the copper in coating form along with external heating from the root side has minimized the temperature gradient and maintains homogenous material flow in the weld zone and increased bond strength.

Keywords Aluminum; Copper inclusion; External heating; FSW; IMC; Mechanical and metallurgical properties.

Introduction

Tylecote had mentioned that "after the temporary eclipse of fusion welding processes, the solid state welding processes are beginning to be considered" [1]. This quote has been indisputably proven by the friction stir welding (FSW) process. FSW was invented by The Welding Institute, Cambridge, U.K., in 1991 [2]. The invention of this process is considered to be a major breakthrough in the welding technology. The process avoids the conventional defects associated with the fusion welding processes. Absence of traditional fusion welding defects, reduced distortion and residual stresses, improved mechanical and metallurgical properties, and generation of fine grains with primary particle fragmentation are the major benefits of FSW as the plates are joined in solid state condition [3, 4]. The process parameters that influence the weld properties in FSW are tool geometry, axial force, rotational speed, traverse speed, and tool tilt angle. Several researchers have reported on FSW of precipitation hardenable and non-heat treatable aluminum alloys with respect to microstructural characterization [5–9] and the influence of welding parameters on mechanical properties [8–10]. Importance has been given to the effect of the process parameters of FSW on hardness, fatigue strength, residual stress, and microstructural evolution [10–15]. Experimental flow visualization studies have been conducted to understand the material flow phenomenon in the weld nugget (WN) zone which is the key factor in bond formation [16–19]. The signatures created by varying the process variables offers insight into the working mechanism of FSW. The metallurgical changes and mechanical properties in WN region depend on material composition, thermomechanical history, welding parameters, plate thickness, cooling rate heat sink, and joint design [20, 21]. Linear and nonlinear optimization tools were used to analyze the FSW process parameters, material flow, and its stress behavior, weld zone temperature for various alloys like aluminum, magnesium, etc. have been widely reported [22–28]. Several aspects of FSW phenomena have been numerically and computationally modeled. Prediction of tensile strength of aluminum alloys by numerical models, failure prediction of weld zone by computational models, torque, power requirements by mathematical models, fatigue crack propagation by finite element method, and mechanical properties calculation by neural network approach have also been reported [29–35]. Several researchers have reported their contributions to tools, process parameters, and materials characterization of the similar and dissimilar weldments, and have analyzed their properties. However, very little information is available on the influence of the temperature gradient on microstructural and mechanical properties of dissimilar friction stir welded joints. [40, 41]. The temperature gradient that exists along the weld cross-section in conventional joints initiates the crack at the root of the retreating side and propagates towards weld failure. This

Received March 14, 2012; Accepted June 23, 2012

Address correspondence to J. Kandasamy, Department of Mechanical Engineering, MVSR Engineering College, Nadergul, Hyderabad 501 510, India; E-mail: kandan_kandan@yahoo.co.in

Table 1.—Measured chemical composition of the raw material (wt%).

Composition	Si	Fe	Cu	Mn	Mg	Zn	Cr	Al
AA7075	0.93	0.47	1.5	0.61	2.62	5.42	0.19	Remaining
AA6061	0.67	0.35	0.32	0.09	0.98	0.02	0.17	Remaining
C10400	99.94 copper + 0.026 Ag							

Table 3.—Physical properties of the raw material.

Alloy	Density g/cm^3	Melting point°C	Elastic modulus GPa	Electrical receptivity Ωm	Thermal conductivity W/mK	Thermal expansion/K
AA7075	2.81	555	70	0.038×10^{-6}	172	46×10^{-6}
AA6061	2.7	652	68.9	0.037×10^{-6}	167	23.6×10^{-6}
C10400	8.94	1083	115	0.172×10^{-6}	388	17×10^{-6}

early failure is due to variation in material flow behavior and difference in microstructural changes caused by the temperature gradient between the top and bottom sides of the weldment. In this aspect, an attempt is made to reduce the temperature gradient and to enhance the weld strength through improved intermetallic compound (IMC) properties by introducing an external element.

Experimental procedure

The base material used in this investigation is 6 mm thick AA7075 and AA6061 aluminum alloy plates. Copper is incorporated as an external inclusion along the faying sides as thin strip (of dimensions $120 \times 6 \times 1$ mm), fine particles (2.386 grams per hole is packed in 24 drilled holes of size $\Phi 3 \times 5.5$ mm near the faying sides), and in coating (electrodeposition of 1 micron thickness) forms. The chemical composition, mechanical properties, and physical properties of the aluminum plates and copper are furnished in Tables 1, 2, and 3, respectively. The workpiece dimensions of the plates to be joined are $120 \times 60 \times 6$ mm. The tool is made of high speed steel with 10% cobalt with a tapering pin as shown in Fig. 1(a) with the optimized design dimensions as tabulated in Table 4 [38]. The welding process parameters used in running the experiments are optimized for maximum weld strength as shown in Table 5 [39]. FSW experiments are performed according to the experimental layout shown in Table 6. The corresponding figures are shown in Figs. 1 to 6 in sequence.

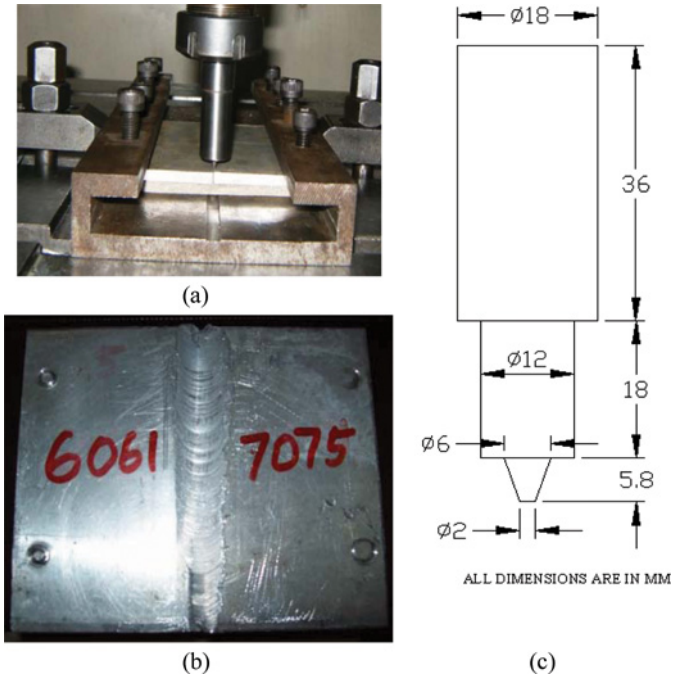

Figure 1.—(a) Fixture, tool, and plates assembly before welding. (b) Conventional weldment. (c) Tool dimensions (color figure available online).

Table 4.—Optimized tool dimensions.

Shoulder diameter (mm)	Pin diameter (mm)	Pin length (mm)
16	6	5.8

Table 5.—Optimized FSW process parameters.

Tool rotational speed (rpm)	Tool travel speed (mm/min)	Axial force (kN)
1,400	16	6

Results and discussions

Hardness

The welded joints were tested for microhardness across the weld direction in Vickers hardness testing machine. A load of 5 kg for 10 s is applied while performing the test. The obtained results are tabulated in Table 7 with the corresponding graphs as shown in Fig. 7. The hardness profile for the conventional weldments show a fall in the Thermo-Mechanically Affected Zone (TMAZ) and subsequently a rise in the weld zone due to the friction processing of the metal and then increase to the base metal hardness. Fall in hardness is noted due to the presence of the existing temperature gradient that supports the flow resistance of the material at the bottom side accompanied by the difference in the tool rotation velocity vector and the tool feed direction vector. The weldments with copper strip and copper particles inclusions

Table 2.—Mechanical properties of the raw material.

Alloy	Tensile strength (MPa)	Yield strength (MPa)	Elongation (%)	Hardness (VHN)	Shear strength (MPa)
AA7075	380	150	12	130	330
AA6061	310	276	17	110	207
C10400	345	310	20	120	195

TABLE 6.—Experimental layout.

Exp. No./Weldment No.	Base material (advancing side)	Externally alloying material (form)	Base material (retreating side)
1	AA7075	Nil	AA6061
2	AA7075	Copper strip (solid form, 1 mm thick strip)	AA6061
3	AA7075	Copper granules in drilled holes, Φ 1 mm (fine particles)	AA6061
4	AA7075	Copper granules in faying sides for 1 mm (fine particles)	AA6061
5	AA7075	Copper coating (coating, 75 microns thick coating)	AA6061
6	AA7075	Copper coating + external heating from root side	AA6061

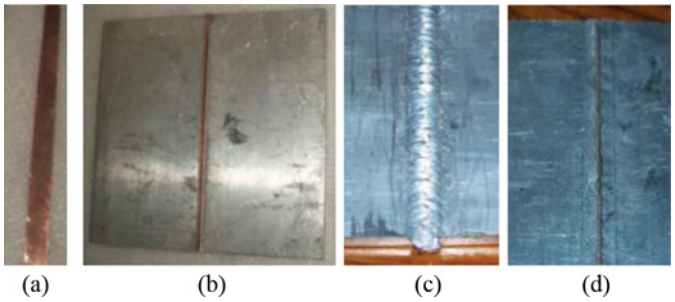

FIGURE 2.—(a) Copper strip. (b) Aluminum plates and copper strip in assembly. (c) Top side. (d) Root side of weldment (color figure available online).

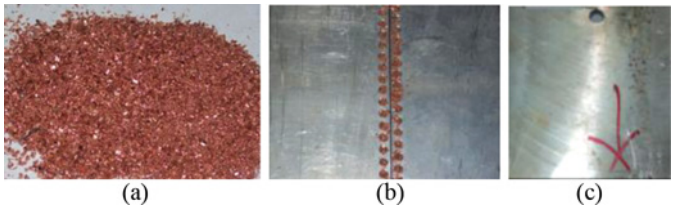

FIGURE 3.—(a) Copper particles. (b) Particles packed in drilled holes. (c) Top side of the weldment (color figure available online).

FIGURE 4.—(a) Copper particles packed in faying sides. (b) Root side of the weldment (color figure available online).

show a rise in hardness in the weld zone as compared to the conventional weldments due to the IMC formed. Unmolded particles of the copper particles on the surface and the adjacent layers in the aluminum matrix resulted in erratic behavior of the microhardness in the proximity

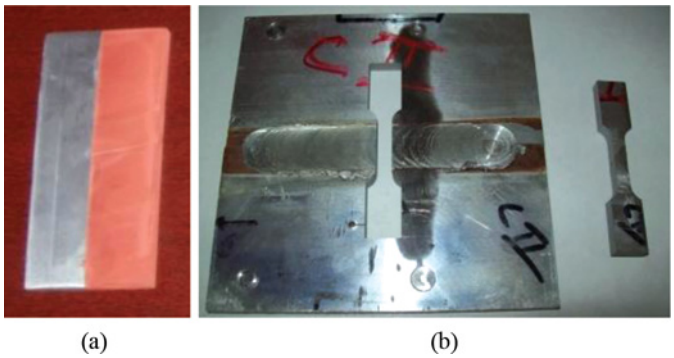

FIGURE 5.—(a) Copper coated aluminum alloy workpiece. (b) Top side of weldment. (c) Extracted tensile test specimen (color figure available online).

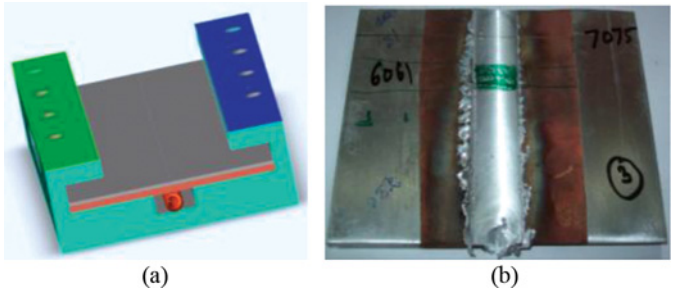

FIGURE 6.—(a) Solid model of the designed fixture with heating element. (b) Weldment exhibiting the temperature effect (color figure available online).

TABLE 7.—Distribution Vickers microhardness across the weld line.

	Distance from the weld nugget (mm)												
	Advancing side						WN	Retreating side					
Weldment No.	−6	−5	−4	−3	−2	−1	0	1	2	3	4	5	6
1	119	115	100	60	55	62	70	64	53	62	108	118	115
2	118	114	107	54	50	69	82	76	61	66	111	116	115
3	120	118	112	57	54	67	77	66	67	67	108	120	114
4	121	113	109	59	63	69	74	68	71	68	112	116	113
5	119	115	110	58	59	66	69	67	65	68	114	118	115
6	118	114	124	59	65	72	70	71	65	60	116	115	116

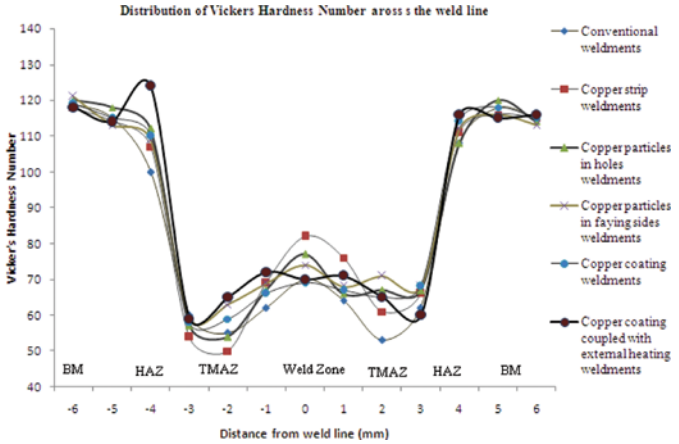

FIGURE 7.—Distribution of Vickers hardness number across the weld line (color figure available online).

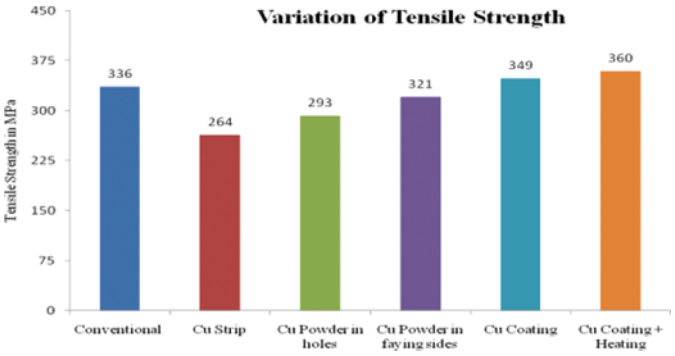

FIGURE 8.—Variation of tensile strength across the weldment for different experimental conditions (color figure available online).

to the weld zone. Coarse grains, improper diffusion, nonhomogenous IMC, different grain size, and phases of the copper particles are the major causes for uneven hardness distribution in the copper particles packed in holes and faying sides weldments. The copper coated weldments exhibit a gradual decrease from the parent metal hardness to TMAZ, varies smoothly from the advancing side to the retreating side with the minimum hardness being observed in the TMAZ. This smooth variation is due to the reduced temperature gradient in the weld cross-section caused by the copper coating and uniform metal flow that led to the formation of homogenous IMC. The copper coated and externally heated weldments reveal that hardness distribution across the weld zone is very smooth as compared to the other weldments due to more uniform metal flow, homogenous IMC formation with time, fine dispersening, and diffusion of the copper coated particles into the aluminum matrix leading to equiaxed smaller grains.

Tensile Strength

Tensile test specimens extracted as per E8 standards are tested in UTM. The results obtained are tabulated in Table 8 and the corresponding graphs are plotted as show in Fig. 8. Reduced value of hardness with coarse grains in the retreating side, nonhomogenity in metal flow due to the existence of temperature gradient between the top and root sides of the weldment led to consistent failure of the conventional joints by crack initiation and propagation on the bottom part of the TMAZ in retreating side. Resistance to material flow caused by the interruption of the inserted copper strip during welding has led to a weak metallurgical bond. Lack of formation of a strong solid solution and irregular distribution of the unmolded copper strip particles in the aluminum matrix in nugget zone led to a weaker IMC and early failure of the joints. Reasonable tensile strength properties were witnessed while testing the extracted tensile test specimens in copper particles packed weldments as compared to conventional weldments. This may be due to the reduction in temperature gradient and a soluble IMC formed in the weld zone. The end result observed in copper coated weldments across the weld direction, supports the hardness results. Uniform flow of the base material throughout the weld cross-section, formation of a strong and homogenous IMC due to reduction in temperature gradient by enhanced thermal conductivity of the copper coating in the weld zone had led to improved weld strength. Tremendously improved tensile properties are observed in externally heated copper coated weldments due to the homogeneous flow rate of the material and the uniform IMC formed across the weldment due to the external heat supplied leaving no chance for the retreating side, root part, TMAZ of the weld as vulnerable as in conventional weldments. The metallurgical bond was equally strong on the top and

TABLE 8.—Tensile strength behavior across the weld direction.

Weldment No.	Tensile strength across weld direction (MPa)	% TS of parent material (AA7075)	% TS of parent material (AA6061)
1	336	88.4	108.4
2	264	69.5	85.2
3	293	77.1	94.5
4	321	84.5	103.5
5	349	91.8	112.6
6	360	94.7	116.1

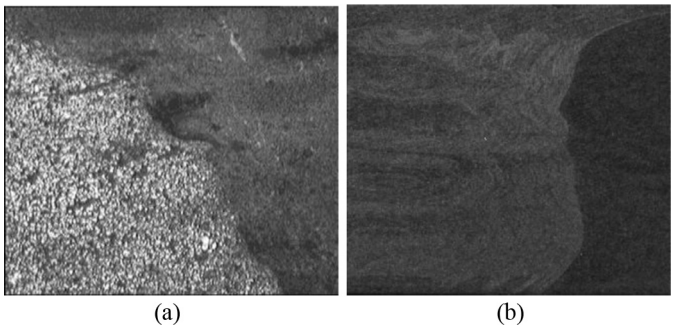

FIGURE 9.—Conventional weldments: (a) boundary line and (b) weld cross-section.

root side of the weld owing to microstructure refinement throughout the weldment volume.

Microstructures

The mechanically polished surfaces of the specimens were chemically etched with Kellers reagent to determine the microstructure of the weldments. Optical microscope with 400× magnification was used to identify the microstructures of the weldments for all conditions. The boundary line in Fig. 9 shows the clear distinction of the base metal and the weld zone which leads to easy failure of the weldment by trouble-free crack formation. The microstructures of the copper inserted weldments show considerable variation due to the inhomogeneous nature of the metal flow in the root part of the retreating side. Substantial difference is observed in the IMC due to irregular dispersion of the copper particles and unmolded and unreacted copper particles in the aluminum matrix. This indicates the direct influence of the formed metallurgical bond on the poor performance in mechanical properties due to the discontinuities observed in the IMC formed on the retreating side as shown in Fig. 10. Microstructures obtained from the copper particles packed weldments indicates smooth transformation of the IMC from aluminum matrix with copper inclusion, with narrow discontinuities of thread-like form in the retreating side as shown in Fig. 11. Similar to conventional weldments, these weldments also represent the variation in microstructures and accordingly the weld strength is varied. Keen observations made on the advancing and retreating side microstructures and tensile test result indicates the start of the crack formation is random in-between the TMAZ of the retreating side to the weld nugget, an indication of improvement, in the failure behavior.

The variation in material flow of copper coated and externally heated copper coated weldments is clearly shown in Fig. 12 and 13, respectively. In both cases, smooth transformation of the aluminum alloys into an intermetallic composition of Al_2Cu and Al_4Cu_9 indicates the even flow of the extruded material from one side into the other side of the welded joint, forming a strong IMC and good metallurgical bond with superior mechanical properties. The crack initiation at the retreating root side in conventional weldments as shown in Fig. 14 indicates the clear possibility of easiness of the joint failure as compared to the externally heated copper coated weldments. Electron diffraction analysis conducted on the IMC formed, as shown in Figs. 15(a),(b), confirms the formation of Al_2Cu and Al_4Cu_9 as IMC in copper coated weldments with equiaxed grains, which enhances the bond strength. External heating has provided uniform metal flow along the cross-section with no chance of unevenness at any stage of bond formation along the weld cross-section. The reduced temperature gradient and the formed IMC have eliminated the chances of defect formation at the root of retreating side.

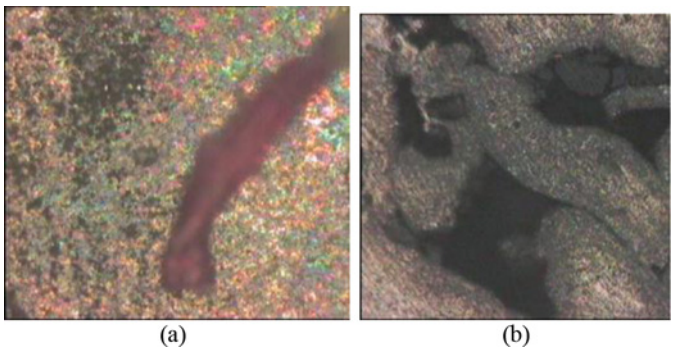

FIGURE 10.—(a) Unmolded copper strip in weld zone. (b) Discontinuities in weldments. Copper strip weldments (color figure available online).

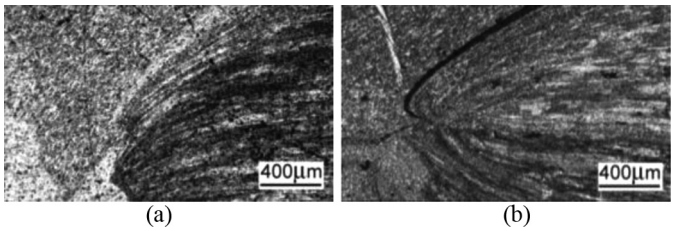

FIGURE 11.—Copper particles weldments: (a) AS and (b) RS.

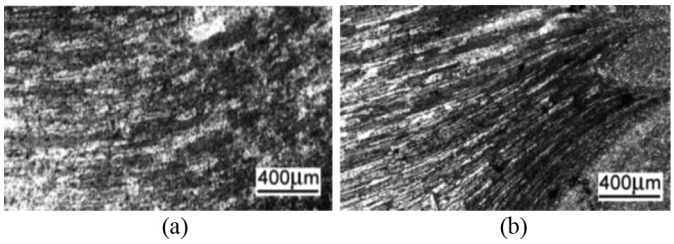

FIGURE 12.—Copper coated weldments: (a) AS and (b) RS.

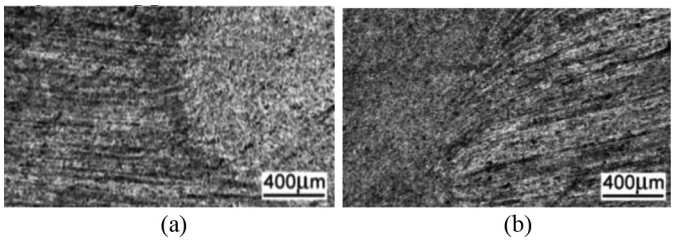

FIGURE 13.—Copper coated coupled with external heating weldments: (a) AS and (b) RS.

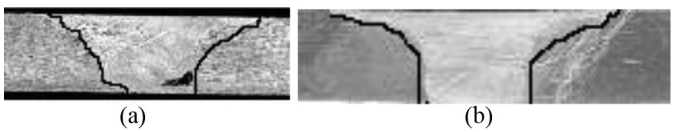

FIGURE 14.—(a) Conventional weldment with crack in the root part of the retreating side. (b) Copper coated and externally heated weldment with no crack.

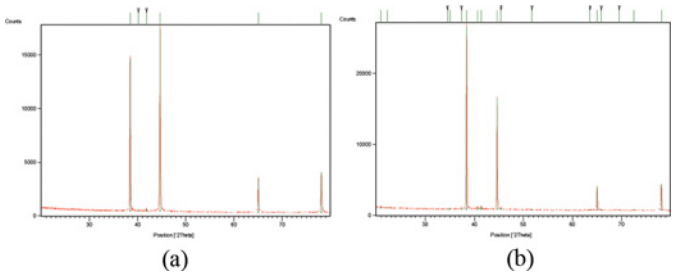

FIGURE 15.—(a) X-ray diffraction of the specimen without copper inclusion. (b) X ray diffraction of the specimen with copper inclusion (color figure available online).

SCANNING ELECTRON MICROSCOPY (SEM) RESULTS

The scanning electron microscopy (SEM) results of the conventional joints in Fig. 16 reveals the kissing bond in the fracture spot, which is a clear indication of lack of frictional heat generated due to difference in heat flow along the cross-section, while forming the weld nugget. Subsequently the metal around the tool could not infuse and effect recrystallization, as it sticks to each other, leading to a kissing bond, a predominant factor for joint failure. The outcome of the SEM analysis of the aluminum alloy joints with copper insert in Fig. 16(b) reveals copper particles in pieces and bits in solid form in the fracture spot. It clearly denotes that the lack of formation of the solid solution and the material is forced layer over the layer to form a pseudo weld nugget. The copper particles packed weldments exhibit plastically deformed, thermally affected and TMAZ. The clear distinction of the zones could not be located due to the flow of particles into the aluminum alloy matrix. SEM analysis of the tensile tested fracture surfaces obtained from the copper coated and externally heated copper coated weldments are shown in Fig. 17. It indicates the presence of long and large voids, small depressions, tear ridges, particle matrix de cohesion, all indicating the possibility of ductile failure. The fracture surfaces show wide distribution of microvoid coalescence revealing ductile behavior of the welded joint before fracture. From the above observations of the fractographic results, it is observed that the copper coated weldments, which has high thermal conductivity makes the joint temperature nearly up to $0.7\,T_m$, measured using temperature sensors, makes the material to flow easily to form a strong metallurgical bond as compared to the sticking nature of material flow in conventional joints.

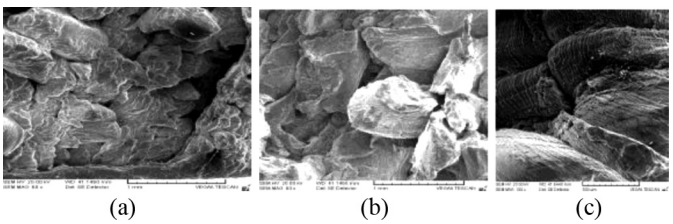

FIGURE 16.—(a) Conventional weldment. (b) Copper strip weldment. (c) Copper particles filled in holes weldment.

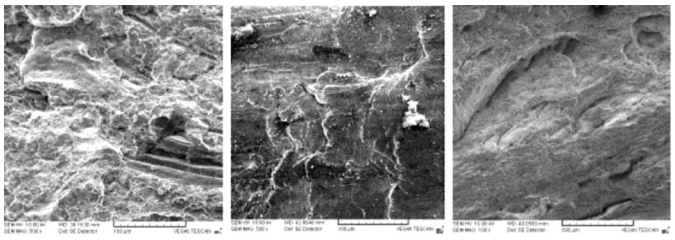

FIGURE 17.—(a) Weldment with copper particles filled in the faying sides. (b) Weldment with copper coating. (c) Weldment with copper coating coupled with external heating.

CONCLUSIONS

1. The copper strip inserted weldments show reduced temperature gradient with reduced weld strength as compared to conventional weldments, due to the nonmelting of copper strip and random distribution of the unreacted copper particles along the cross-section and weld line.
2. The copper particles packed in holes and in the faying sides weldments have shown marginal improvement in mechanical properties as compared to the copper strip inserted weldments, due to uniform metal flow along the cross section due to reduced temperature gradient. The reduction in strength as compared to conventional weldments is due to loss of material by drilling and the outflow of the particles from the faying sides caused by the tool rotational speed.
3. The copper coated weldments have shown considerably good mechanical and metallurgical properties due to uniform metal flow along the cross-section.
4. The copper coated weldments with external heating from bottom side have shown excellent weld properties as compared to all the other weldments due to the elimination of the temperature gradient and homogenous metal flow, formation of a strong IMC, and hence the weld joint.
5. Mechanical and metallurgical investigations on the IMC formed revealed that a sound weldment in FSW with improved properties is possible by introducing a copper coating on the faying sides of the weld plates with external heating from the root side.
6. The coating thickness may be optimized on the faying sides in the tool–workpiece contact area, for the maximum possible conduction of the heat generated on the top side of the weldment towards the cross section for uniform metal flow.

REFERENCES

1. Tylecote, R.F. *The Solid Phase Welding of Metals*; Edward Arnold: London, 1968.

2. Thomas, W.M.; Nicholas, E.D.; Needham, J.C.; Church, M.G.; Templesmith, P.; Dawes, C.J. Friction stir welding. International patent application no. PCT/GB92102203. Great Britain application no. 9125978.8, 1991.
3. Thomas, W.M.; Nicholas, E.D. Friction stir welding for the transportation industries. *Mater. Des.* **1997**, *18*, 269–273.
4. Mandal, N.R. *Aluminum Welding*; second ed.; Narosa: New Delhi, India, 2005.
5. Jata, K.V.; Shankaran, K.K.; Ruschau, J.J. Friction-stir welding effects on microstructure and fatigue of aluminum alloy 7050-T7451. *Metall. Mater. Trans. A* **2003**, *31A*, 2181–2192.
6. Su, J.Q.; Nelson, T.W.; Mishra, R.; Mahoney, M. Microstructural investigation of friction stir welded 7050-T651 aluminum. *Acta. Mater.* **2003**, *51A* (3), 713–729.
7. Sato, Y.S.; Park, S.H.C.; Kokawa, H. Microstructural factors governing hardness in friction stir welds of solid–solution-hardened Al alloys. *Metallurgical and Materials Transactions A* **2001**, *32*, 3033–3042.
8. Sato, Y.S.; Urata, M.; Kokawa, H. Parameters controlling microstructure and hardness during friction-stir welding of precipitation-hardenable aluminum alloy 6063. *Metall. Mater. Trans. A* **2002**, *33A*, 625–635.
9. Rhodes, C.G.; Mahoney, M.W.; Bingel, W.H.; Calabree, M. Fine grain evolution in friction stir processed 7050 aluminum. *Scripta Materialia* **2003**, *48*, 1451–1455.
10. Liu, H.J.; Fujii, H.; Maeda, M.; Nogi, K. Tensile properties and fracture locations of friction-stir welded joints of 2017-T 351 aluminum alloy. *Journal of Material Processing Technology* **2003**, *142* (3), 692–696.
11. Liu, H.J.; Fujii, H.; Maeda, M.; Nogi, K. Tensile properties and fracture locations of friction-stir welded joints of 6061-T6 aluminum alloy. *Journal of Material Processing Technology* **2003**, *22* (15), 1061–1063.
12. Zaw, S.R.; Ma, Z.Y.; Chew, L.Q. Effect of parameters on tensile properties and fracture behaviour of friction Stir Welded Al-Mg-Si alloy. *Scripta Materialia* **2007**, *56*, 69–72.
13. Kato, K.; Tikisu, H.; Ito, G. Mechanical properties of friction stir welded 6061 aluminum alloy. *Welded International* **2004**, *18*, 95–102.
14. Cavaliere, P.; Cabibo, M.; Panella, F.; Squillace, A. 2198 Al–Li plates joined by friction stir welding: mechanical and microstructural behaviour. *Materials and Design* **2009**, *30*, 3622–3631.
15. Chen, Y.C.; Nakata, K. Microstructural characterization and mechanical properties in friction stir welding of aluminum and titanium dissimilar alloys. *Materials and Design* **2009**, *30*, 469–474.
16. Colligan, K. Material flow behaviour during friction stir welding of aluminum. Welding research supplement. *Welding Journal* **1999**, 229s–237s.
17. Hamilton, C.; Dymek, S.; Blicharski, M. A model of material flow during friction stir welding. *Materials Characterization* **2008**, *59*, 1206–1214.
18. Leal, R.M.; Leitao, C.; Loureiro, A.; Rodrigues, D.M.; Vilaca, P. Material flow in heterogeneous friction stir welding of thin aluminum sheets: Effect of shoulder geometry. *Materials Science and Engineering* **2008**, *498*, 384–391.
19. Kumar, K.; Kailas, S.V. The role of friction stir welding tool on material flow and weld formation. *Materials Science and Engineering* **2008**, *485*, 367–374.
20. Sato, Y.S.; Kokawa, H.; Enmoto, M.; Jogan, S. Microstructural evolution of 6063 aluminum during friction stir welding. *Metallurgical Materials Transactions* **1999**, *30*, 2429–2436.
21. Sato, Y.S.; Kokawa, H. Distribution of tensile property and microstructure in friction stir weld of 6063 aluminum. *Metallurgical and Materials Transactions A* **2001**, *32*, 3023–3031.
22. Vijayan, S.; Raju, R. Process parameter optimization and characterization of friction stir welding of aluminum alloys. *Journal of Applied Engineering Research* **2008**, *3* (10), 1303–1316.
23. Vijayan, S.; Raju, R.; Subbaiah, K.; Sridhar, N.; Rao, S.R.K. Friction stir welding of Al–Mg alloy optimization of process parameters using Taguchi method. *Experimental Techniques, Society for Experimental Mechanics* **2008**, *34* (5), 37–44.
24. Babu, S.; Elangovan, K.; Balasubramanian, V.; Balasubramanian, M. Optimizing friction stir welding parameters to maximize tensile strength of AA2219 aluminum alloy joints. *Journal of Metallurgy and Material Science* **2009**, *15* (2), 321–330.
25. Jayaraman, M.; Sivasubramanian, R.; Balasubramanian, V.; Lakshminarayanan, A.K. Optimization of process parameters for friction stir welding of cast aluminum alloy A319 by Taguchi method. *Journal of Scientific and Industrial Research* **2009**, *68*, 36–43.
26. Record, J.H.; Covington, J.L.; Nelson, T.W.; Sorensen, C.D.; Webb, B.W. A look at the statistical identification of critical process parameters in friction stir welding, Welding research supplement. *Welding Journal*, 97s–103s.
27. Rajamanickam, N.; Balusamy, V. Effects of process parameters on mechanical properties of friction stir welds using design of experiments. *Indian Journal of Engineering & Materials Sciences* **2008**, *15*, 293–299.
28. Ozerdem, M.S.; Kolukisa, S. Artificial neural network approach to predict the mechanical properties of Cu-Sn-Pb-Zn-Ni cast alloys. *Materials and Design* **2009**, *30*, 764–769.
29. Balasubramanian, V. Relationship between base material properties and friction stir welding process parameters. *Materials Science and Engineering* **2008**, *480*, 397–403.
30. Liechty, B.C.; Webb, B.W. Modeling the frictional boundary condition in friction stir welding. *International Journal of Machine Tools and Manufacture* **2008**, *48*, 1474–1485.
31. Ozerdem, M.S.; Kolukisa, S. Artificial neural network approach to predict the mechanical properties of Cu-Sn-Pb-Zn-Ni cast alloys. *Materials and Design* **2009**, *30*, 764–769.
32. Golestaneh, A.F.; Ali, A.; Zadeh, M. Modelling the fatigue crack growth in friction stir welded joint of 2024-T351 Al alloy. *Materials and Design* **2009**, *30*, 2928–2937.
33. Arora, A.; Nandan, R.; Reynolds, A.P. Deb Roy, T. Torque, power requirement and stir zone geometry in friction stir welding through modeling and experiments. *Scripta Materialia* **2009**, *60*, 13–16.
34. Zadpoor, A.A.; Sinke, J.; Benedictus, R. Finite element modeling and failure prediction of friction stir welded blanks. *Materials and Design* **2009**, *30*, 1423–1434.
35. Elangovan, K.; Balasubramanian, V.; Babu, S. Predicting tensile strength of friction stir welded AA6061 aluminum alloy joints by a mathematical model. *Materials and Design* **2009**, *30*, 188–193.
36. Zhang, Z.; Zhang, H.W. Numerical studies on controlling of process parameters in friction stir welding. *Journal of Material Processing Technology* **2009**, *209*, 241–270.

37. Chen, Y.C.; Nakata, K. Effect of tool geometry on microstructure and mechanical properties of friction stir lap welded magnesium alloy and steel. *Materials and Design* **2009**, *30*, 3913–3919.
38. Kandasamy, J.; Govindaraju, M.; Manzoor Hussain, M.; Rajesham, S. Design, manufacture and analysis of a friction stir welding tool to join aluminum 6 series alloys. In *Proceedings of the International Conference on Intelligent Design and Analysis of Engineering Products, Systems and Computation*, Sri Krishna College of Engineering and Technology, Coimbatore, India, July 9–10, 2010.
39. Kandasamy, J.; Govindaraju, M.; Manzoor Hussain, M.; Rajesham, S. Dissimilar friction stir welds in aluminum alloys: Optimization of the process parameters for tensile strength and metallurgical characterization. *Technology Spectrum: Journal of Jawaharlal Nehru Technological University Hyderabad* **2010**, *4* (2), 43–51.
40. Mishra, R.S.; Ma, Z.Y. Friction stir welding and processing. *Materials Science and Engineering* **2005**, *50*, 1–78.
41. Nandan, R.; Roy, G.G.; Lienert, T.J.; Deb Roy, T. Numerical modelling of 3D plastic flow and heat transfer during friction stir welding of stainless steel. *Science and Technology of Welding and Joining* **2006**, *11* (5), 526.
42. Akinlabi, E.T.; Els-Botes, A.; Lombard, H. Effect of tool displacement on defect formation in friction stir welding of aluminum and copper. In *Proceedings of the 8th International Friction Stir Welding Symposium*, Hamburg, Germany, May 18–20, 2010.
43. Adamowski, J.; Szkodo, M. Friction stir welds (FSW) of aluminum alloy AW6082-T6. *Journal of Achievements in Materials and Manufacturing Engineering* **2007**, *20*, 403–406.
44. Shanmuga Sundaram, N.; Murugan, N. Tensile behavior of dissimilar friction stir welds of aluminum alloys. *Materials and Design* **2010**, *31*, 4184–4193.